Molecular Therapy
Nucleic Acids
Original Article

m^{6}A Methylation of Precursor-miR-320/RUNX2 Controls Osteogenic Potential of Bone Marrow-Derived Mesenchymal Stem Cells

Gege Yan,[3,4] Ye Yuan,[2,3,4] Mingyu He,[3,4] Rui Gong,[3] Hong Lei,[3] Hongbao Zhou,[1] Wenbo Wang,[1] Weijie Du,[3] Tianshuai Ma,[3] Shenzhen Liu,[3] Zihang Xu,[3] Manqi Gao,[3] Meixi Yu,[3] Yu Bian,[3] Ping Pang,[3] Xin Li,[3] Shuting Yu,[3] Fan Yang,[3] Benzhi Cai,[2,3] and Lei Yang[1]

[1]Department of Orthopedics, The First Affiliated Hospital of Harbin Medical University, Harbin 150001, China; [2]Department of Pharmacy, The Second Affiliated Hospital of Harbin Medical University, Harbin, China; [3]Department of Pharmacology, College of Pharmacy, Harbin Medical University, Harbin 150081, China

Methyltransferase-like 3 (METTL3) is the main enzyme for *N*^{6}-methyladenosine (m^{6}A)-based methylation of RNAs and it has been implicated in many biological and pathophysiological processes. In this study, we aimed to explore the potential involvement of METTL3 in osteoblast differentiation and decipher the underlying cellular and molecular mechanisms. We demonstrated that METTL3 is downregulated in human osteoporosis and the ovariectomized (OVX) mouse model, as well as during the osteogenic differentiation. Silence of METTL3 by short interfering RNA (siRNA) decreased m^{6}A methylation levels and inhibited osteogenic differentiation of bone marrow-derived mesenchymal stem cells (BMSCs) and reduced bone mass, and similar effects were observed in METTL3$^{+/-}$ knockout mice. In contrast, adenovirus-mediated overexpression of METTL3 produced the opposite effects. In addition, METTL3 enhanced, whereas METTL3 silence or knockout suppressed, the m^{6}A methylations of runt-related transcription factor 2 (RUNX2; a key transcription factor for osteoblast differentiation and bone formation) and precursor (pre-)miR-320. Moreover, downregulation of mature miR-320 rescued the decreased bone mass caused by METTL3 silence or METTL3$^{+/-}$ knockout. Therefore, METTL3-based m^{6}A modification favors osteogenic differentiation of BMSCs through m^{6}A-based direct and indirect regulation of RUNX2, and abnormal downregulation of METTL3 is likely one of the mechanisms underlying osteoporosis in patients and mice. Thus, METTL3 overexpression might be considered a new approach of replacement therapy for the treatment of human osteoporosis.

INTRODUCTION

*N*6-methyladenosine (m^{6}A) has been thought of as the most abundant modification of messenger RNAs (mRNAs) or non-coding RNAs in eukaryotes since the 1970s when it was discovered.[1–3] The key components of the m^{6}A methyltransferase complex have been recently identified, including WTAP (Wilms tumor 1-associated protein), methyltransferase-like 3 (METTL3), and METTL14, as well as m^{6}A demethylase, including FTO (fat mass and obesity-associated protein) and ALKBH5 (ALKB homolog 5).[4,5] Cytoplasmic METTL3 contains an active methyltransferase domain that plays a pivotal role in catalyzing conversion of adenosine (A) to m^{6}A.[2] It is known that m^{6}A modification exerts diverse biological functions.[6] FTO as an m^{6}A RNA demethylase acts as an oncogenic factor in acute myeloid leukemia (AML) and regulates cardiac function in the development of heart failure by reducing the m^{6}A mRNA level.[7,8] METTL14 interacts with the microprocessor protein DGCR8 and positively modulates primary (pri-)miR-126 processing in an m^{6}A-dependent manner during tumor progression of hepatocellular carcinoma.[9]

Over the last decade, interest in stem cell-based therapies from both fundamentalists and clinicians has been overwhelming because of the great potential and promise of these strategies for the treatment of human diseases.[10–12] Especially, bone marrow-derived mesenchymal stem cells (BMSCs) have been reported to favor osteogenic differentiation and correct the imbalance of bone metabolism.[13–15] It would be of great interest and paramount importance to know whether m^{6}A modification can affect translation of osteogenic genes and mRNAs or non-coding RNAs in BMSCs. Herein, we report that METTL3-induced m^{6}A methylation of RNAs promotes osteogenic differentiation of BMSCs through m^{6}A-based post-transcriptional regulation of runt-related transcription factor 2 (RUNX2), a key factor involved in osteogenesis.

Received 27 May 2019; accepted 3 December 2019;
https://doi.org/10.1016/j.omtn.2019.12.001.

[4]These authors contributed equally to this work.

Correspondence: Lei Yang, Department of Orthopedics, The First Affiliated Hospital of Harbin Medical University, Harbin 150001, China.
E-mail: yangray83@vip.qq.com
Correspondence: Benzhi Cai, Department of Pharmacy, The Second Affiliated Hospital of Harbin Medical University, Harbin, China.
E-mail: caibz@ems.hrbmu.edu.cn
Correspondence: Ye Yuan, Department of Pharmacy, The Second Affiliated Hospital of Harbin Medical University, Harbin, China.
E-mail: yuanye_hmu@126.com

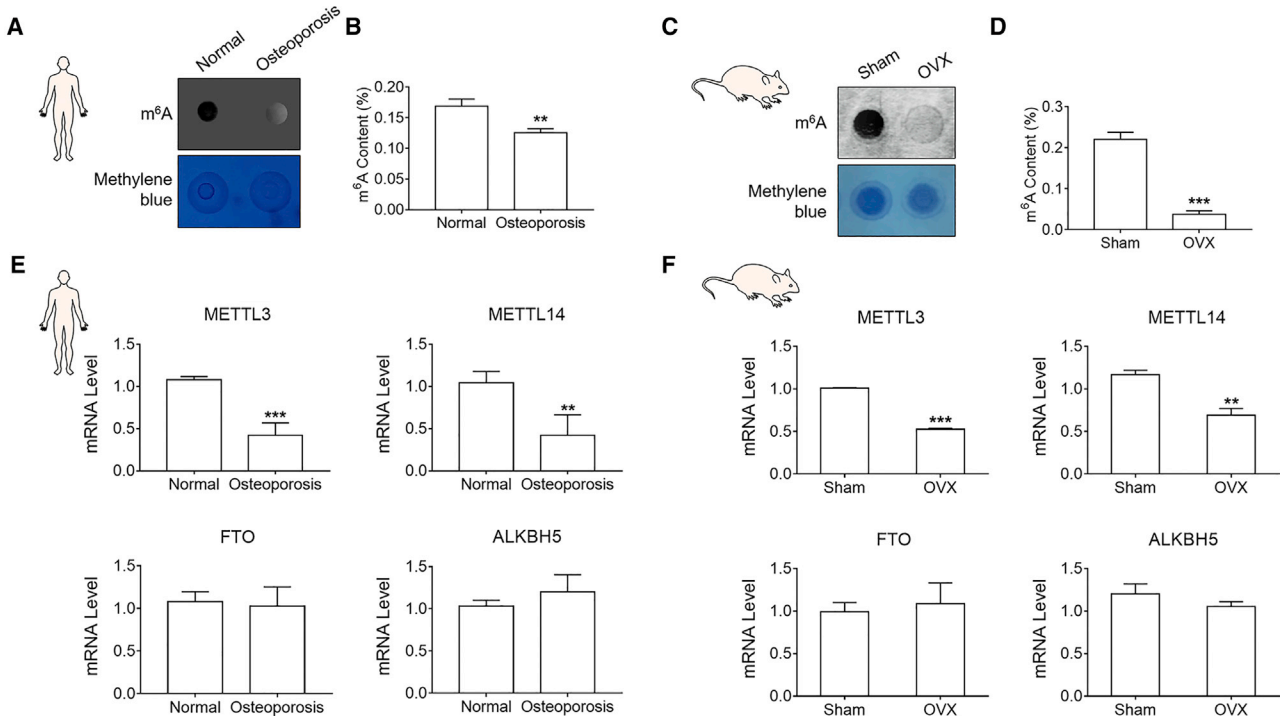

Figure 1. Decreases in Global m^{6}A Level and METTL3 Expression in Osteoporosis Bone Tissues

(A and B) Decreases of global m^{6}A levels in total RNAs isolated from bone tissues of patients with osteoporosis compared with those of healthy subjects. m^{6}A modification of RNAs was determined by m^{6}A dot blot analysis (A) and an m^{6}A ELISA kit (B). n = 3. (C and D) Decrease of global m^{6}A level in bone tissues of OVX mice with osteoporosis relative to that in sham-operated control counterparts. n = 4. (E and F) Expression downregulation of m^{6}A methyltransferases METTL3 and METTL14 mRNAs in bone tissues from osteoporosis patients (E) and OVX mice (F) relative to those from healthy human subjects and sham control mice, respectively. In comparison, the transcript levels of demethylases FTO and ALKBH5 were not different between osteoporosis and controls. mRNA levels were determined by qRT-PCR. Data are expressed as mean ± SEM. *p < 0.05, **p < 0.01, ***p < 0.001. n = 4.

RESULTS

METTL3 and m^{6}A Modification Are Decreased in Osteoporosis

Osteoporosis is characterized by low bone mass, decline of bone quality, and microarchitectural deterioration, leading to increases in fracture and osteopsathyrosis.[16] We quantified m^{6}A contents in total RNAs by RNA dot blot analysis and ELISA assays and examined the expression patterns of m^{6}A methyltransferases METTL3 and METTL14, as well as demethylases FTO and ALKBH5, in bone tissue of patients with osteoporosis and in a mouse model of osteoporosis created by ovariectomized (OVX) mice, as compared to non-osteoporosis human subjects and sham-operated (sham) control mice, respectively. We first confirmed that the expression levels of osteoblast differentiation markers BGLAP, BMP2, Col1a1, and alkaline phosphatase (ALP) were lower in osteoporosis patients and OVX mice than the normal levels in their corresponding control groups (Figures S1 and S2). Meanwhile, m^{6}A contents in total RNA were significantly decreased in bone tissues of both osteoporosis patients (Figures 1A and 1B) and OVX mice (Figures 1C and 1D), as compared to those in their respective control groups. Moreover, there were significant decreases in methyltransferase METTL3 and METTL14 mRNAs, but not in FTO and ALKBH5 (Figures 1E and 1F).

METTL3 Overexpression Promotes Bone Formation

To determine whether METTL3 is a direct regulator of m^{6}A-mediated methylation of mRNAs during bone formation, we used an adenoviral gene delivery system for overexpressing METTL3 through intramuscular injection into C57BL/6 mice (Figure 2A). As shown in Figure 2B, the METTL3 level was markedly increased on both mRNA and protein expression levels in bone tissue in METTL3-overexpressing (OE) mice. Microcomputed tomography (μ-CT) scans revealed that bone mass and bone formation were both remarkably decreased in osteoporotic femur, along with reduced bone mineral density (BMD), trabecular number (Tb.N), trabecular thickness (Tb.Th), and bone volume per tissue volume (BV/TV), as well as increased trabecular separation (Tb.Sp) in the femoral trabecular bone, after 8 weeks in OVX mice compared to those in sham mice. As shown in Figures 2C and 2D, bone mass was significantly decreased in OVX mice, which was partially rescued by METTL3 overexpression. These detrimental alterations were also indicated by hematoxylin and eosin (H&E) staining (Figure 2E).

We next established a METTL3 knockdown mice model using the CRISPR/Cas9 system to investigate the role of METTL3 inhibition

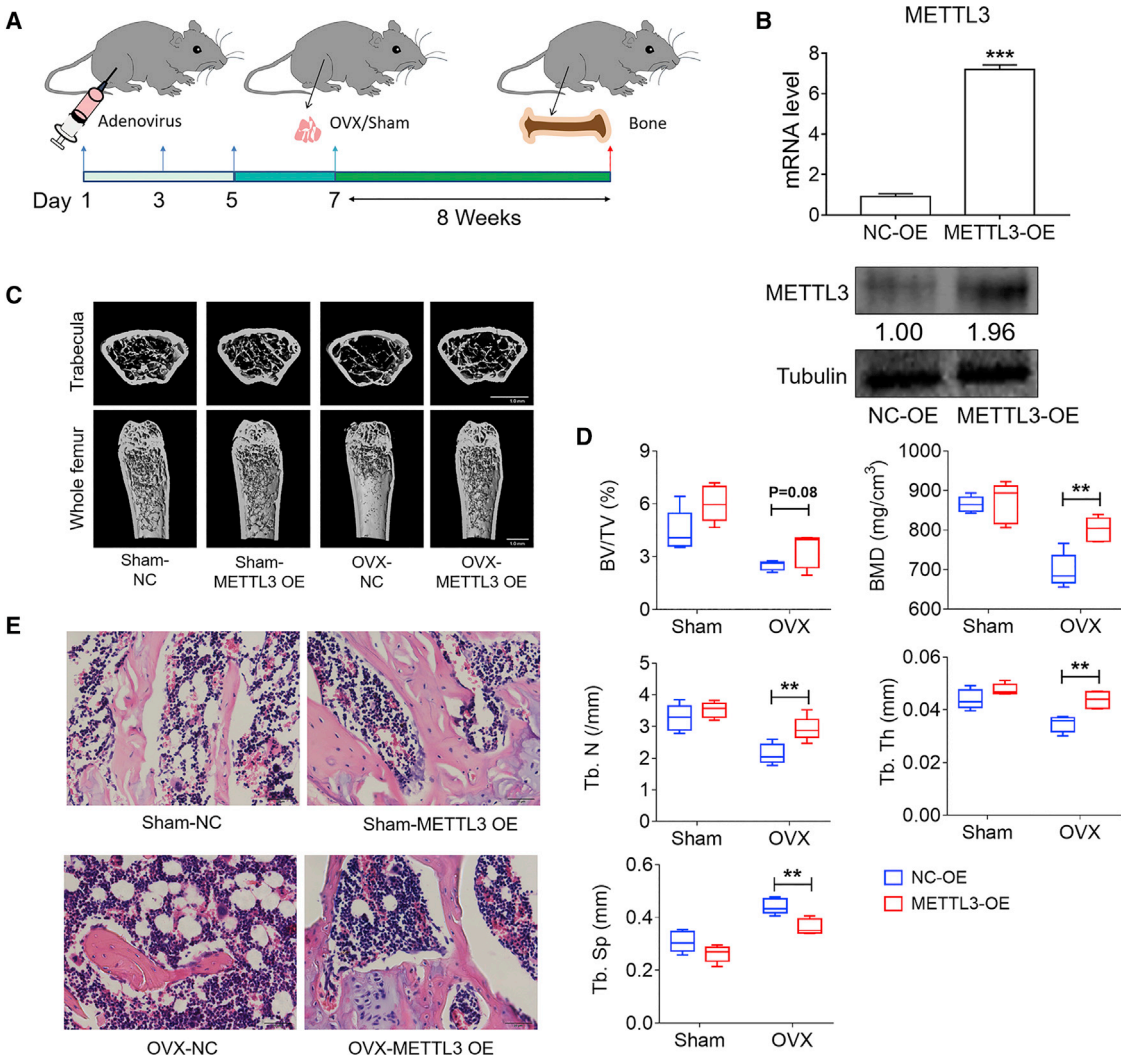

Figure 2. Overexpression of METTL3 Rescues Impaired BMSC Function in OVX Mice

(A) Illustration of experimental protocols for the creation of osteoporosis mice by ovariectomy and administration of METTL3-carrying adenovirus (METTL3-OE) or the empty vector-carrying adenovirus (NC-OE) to OVX mice and sham-operated control counterparts. (B) Verification of the efficiency of METTL-OE to induce METTL3 overexpression at the mRNA (upper, n = 5) and protein (lower) level on day 7 after adenovirus injection in mice. (C) Representative μ-CT images of trabecular bone of the femoral metaphysis (top) and entire proximal femur (bottom) showing the rescuing effects of METTL3-OE on the impaired bone microstructure in OVX mice. Scale bars, 10 mm. (D) μ-CT analysis of femur from 4-month-old females showing the rescuing effects of METTL3-OE on bone volume/tissue volume ratio (BV/TV), bone mineral density (BMD), trabecular number (Tb.N), trabecular thickness (Tb.Th), and trabecular separation (Tb.Sp). n = 5. (E) Representative images of H&E staining of mouse femurs showing the ameliorating effects of METTL3-OE on the reduction of bone formation in OVX mice relative to the sham-control counterparts. Data are expressed as mean ± SEM. *$p < 0.05$, **$p < 0.01$, ***$p < 0.001$. n = 5.

on bone formation (Figure 3A). The efficient knockout of METTL3 expression was confirmed on both mRNA and protein expression levels in bone tissue of the METTL3 heterozygous knockout ($METTL3^{+/-}$) mice (Figure 3B). It has been proven that METTL3 knockout preimplantation epiblasts and naive embryonic stem cells (ESCs) lead to early embryonic lethality.[17] As shown in Figures 3C and 3D, similar results were observed that single METTL3 knockdown exhibited no significant effects on bone formation performed by μ-CT scans. However, METTL3 inhibition significantly further decreased bone mass in OVX mice. It was also shown in H&E staining (Figure 3E). Taken together, these results suggest that METTL3 inhibition reduced bone formation.

Induction of Osteogenic Differentiation of BMSCs by METTL3-Dependent m^6A Methylation of RNAs Underlies Bone Formation

While the above data indicate that METTL3 and m^6A play key roles in bone formation and that expression downregulation of METTL3/m^6A contributes critically to osteoporosis, the underlying mechanisms remained unclear. We proposed that the METTL3-dependent m^6A methylation accounts for bone formation.

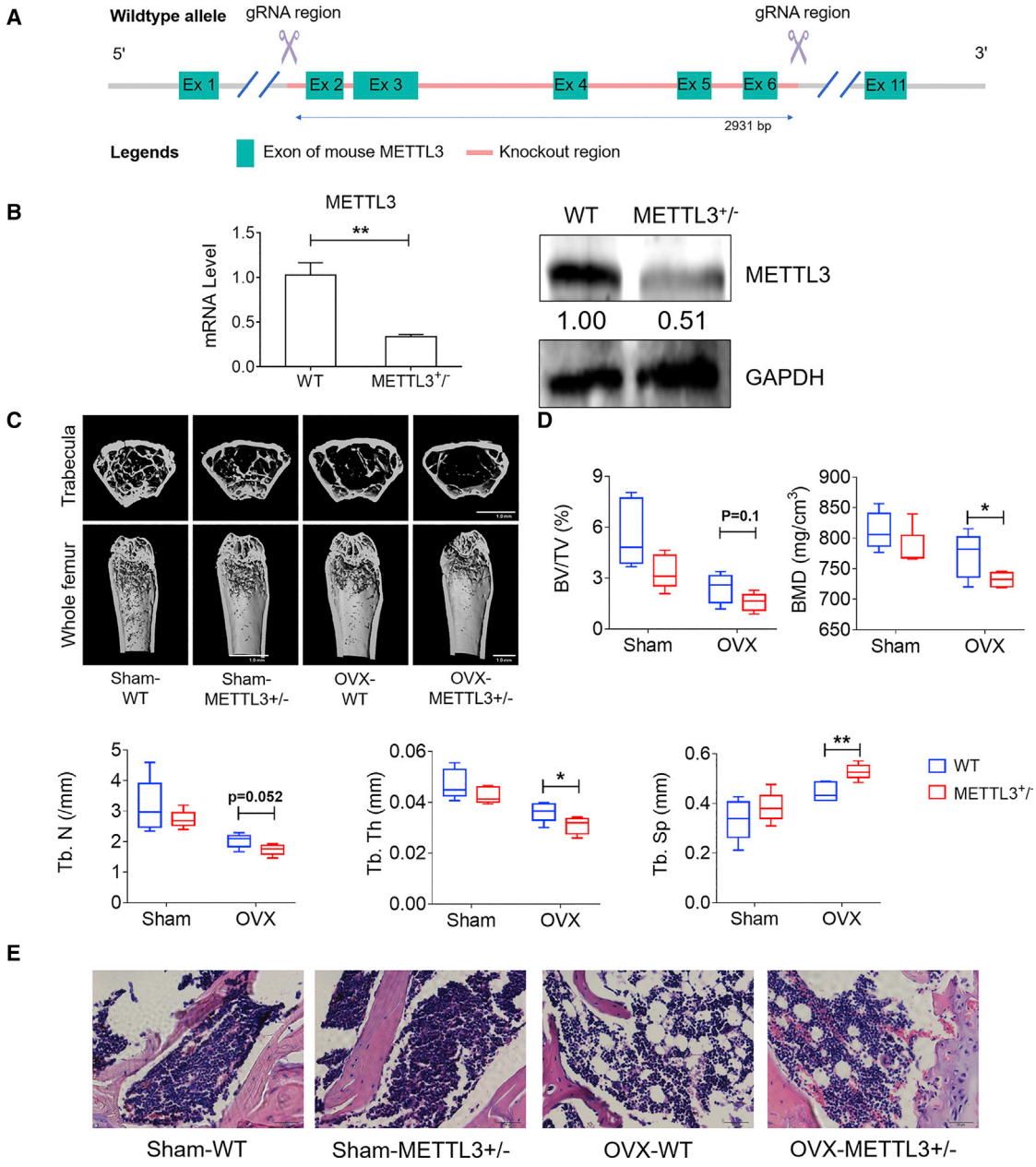

Figure 3. Negative Impact of METTL3 Knockout on Bone Mass and Density

(A) Schematic illustration of generation of METTL3$^{+/-}$ knockout (KO) mice (C57BL/6N) by CRISPR/Cas9-mediated genome engineering strategy. Eleven exons were identified, with the ATG start codon in exon 1 and the TAG stop codon in exon 11. Exons 2–6 were selected as the target site. Cas9 and guide RNA (gRNA) were co-injected into fertilized eggs for mouse production. (B) Verification of the efficiency of CRISPR/Cas9-mediated deletion of METTL3 at the mRNA (left) and protein (right) level on day 7 after adenovirus injection in mice. (C) μ-CT images of trabecular bone of the femoral metaphysis (upper panels) and entire proximal femur (lower panels) showing the impairment of bone microstructure in METTL3$^{+/-}$ mice without ovariectomy and the enhanced impairment of bone microstructure in METTL3$^{+/-}$ mice with ovariectomy. n = 5. (D) μ-CT analysis showing the deceases in BV/TV, BMD, Tb.N and Tb.Th and an increase in Tb.Sp in OVX METTL3$^{+/-}$ mice. n = 5. (E) H&E staining depicting the declined bone formation in METTL3$^{+/-}$ mice with or without ovariectomy compared to the wild-type mice. Data are expressed as mean ± SEM. *p < 0.05, **p < 0.01. n = 5.

We first explored whether METTL3 overexpression (METTL3-OE) regulates osteogenic potential and capacity of BMSCs. Our data demonstrated that METTL3-OE increased m^{6}A levels in total RNAs (Figure 4A). Overexpression of METTL3 in METTL3-OE-treated BMSCs was verified on days 2 and 14 after transfection (Figures 4B and 4C). The expression levels of osteogenic differentiation-related marker genes, including RUNX2, BGLAP, and ALP, were all upregulated on days 7 and 14 during the osteogenic

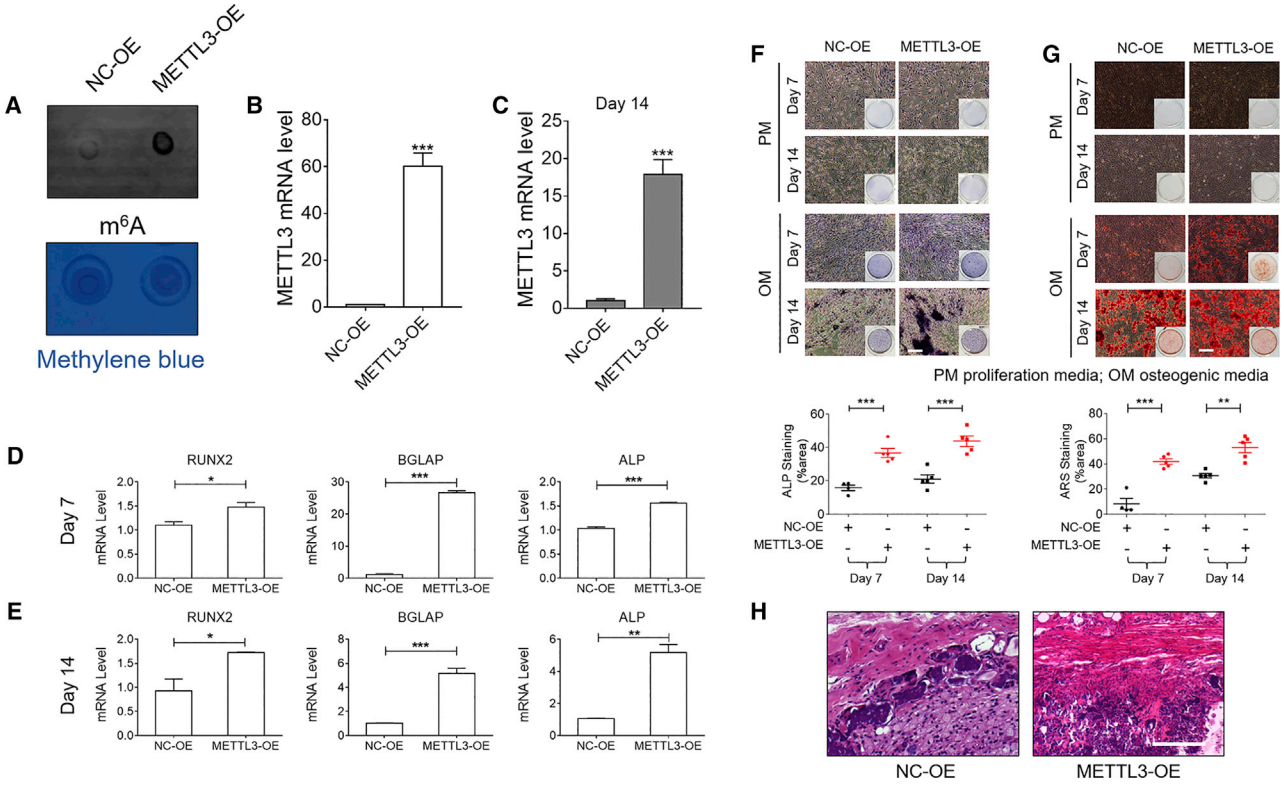

Figure 4. Overexpression of METTL3 Promotes Osteogenic Differentiation of BMSCs

(A) METTL3 overexpression increased m^{6}A content in total RNAs of BMSCs as revealed by m^{6}A dot blot assay. n = 3. (B) Verification of METTL3 overexpression at the mRNA level in BMSCs transfected with METTL3-OE, as detected by qPCR. n = 4. (C) qRT-PCR results showing METTL3 mRNA level on day 14 after transfection with METTL3 plasmid in BMSCs, which cultured with normal complete medium. (D and E) Enhancing effects of METTL3 overexpression on the expression levels of RUNX2, BGLAP, and ALP mRNAs in BMSCs on day 7 (D) and day 14 (E) after transfection of METTL3-OE relative to NC-OE. n = 3. (F) Typical examples of ALP staining (top and middle panels) showing the promoting effect of METTL3 overexpression by METTL-OE on osteogenic differentiation of BMSCs cultured in osteogenic medium. Statistical data (bottom panel) show the increased ALP activities by METTL3-OE relative to NC-OE, as indicated by the elevated percentage of stained area. Scale bar, 150 μm, n = 6. (G) Typical examples of ARS staining (top and middle panels) showing the facilitating action of METTL3 on osteogenic differentiation of BMSCs cultured in osteogenic medium as indicated by enhanced extracellular matrix mineralization (EMM). Statistical data (lower panel) show the increased EMM by METTL3-OE relative to NC-OE, as indicated by the elevated percentage of the stained area. Scale bar, 150 μm, n = 6. (H) Representative H&E staining showing the favorable effects of adenovirus carrying METTL3 gene (METTL3-OE) on bone formation of BMSCs implanted into the back of nude mice, as compared with empty vector (NC-OE) for NC. Scale bars, 50 μm. Data are expressed as mean ± SEM. *p < 0.05, **p < 0.01, ***p < 0.001. n = 3.

differentiation process of BMSCs (Figures 4D and 4E). Furthermore, ALP activity assay and alizarin red staining (ARS) for extracellular matrix mineralization (EMM) were employed for analyzing osteogenic differentiation of BMSCs on days 7 and 14 during the process of differentiation. In this study, we cultured BMSCs in either normal proliferation medium (PM) or osteogenic medium (OM). As shown in Figures 4F and 4G, no difference was observed in PM-cultured BMSCs, but METTL3-OE facilitated osteogenesis of BMSCs, as indicated by both ALP and ARS staining. Similarly, H&E staining revealed that the area of bone formation was significantly higher in the METTL3-OE group than in the control group (Figure 4H).

We then continued our study with loss-of-function approaches. BMSCs can self-renew and differentiate into several distinct cell lineages, including osteoblasts exhibiting induced osteogenesis.[17,18] As depicted in Figure S3, the expression of osteogenesis-associated genes RUNX2, BGLAP, and ALP was increased during the osteogenic differentiation process of BMSCs. Consistently, m^{6}A content in total RNA and METTL3 expression were also robustly increased on days 7 and 14 (Figures 5A and 5B). The levels of demethylase FTO and ALKBH5 remained unchanged (Figure S4). Silence of METTL3 by short interfering RNA (siRNA) (siMETTL3) substantially reduced the degree of m^{6}A modification (Figures 5C and 5D). Efficient silence of METTL3 expression by siMETTL3 was confirmed on day 14 (Figure 5E). Moreover, silence of METTL3 significantly inhibited the expression of osteogenesis-associated genes RUNX2, BGLAP, and ALP during the osteogenic differentiation process of BMSCs (Figure 5F). Furthermore, ALP activity was significantly decreased in BMSCs transfected with siMETTL3 (Figure 5G), as was EMM (Figure 5H). Examination of ectopic bone formation of BMSCs in nude mice using H&E staining

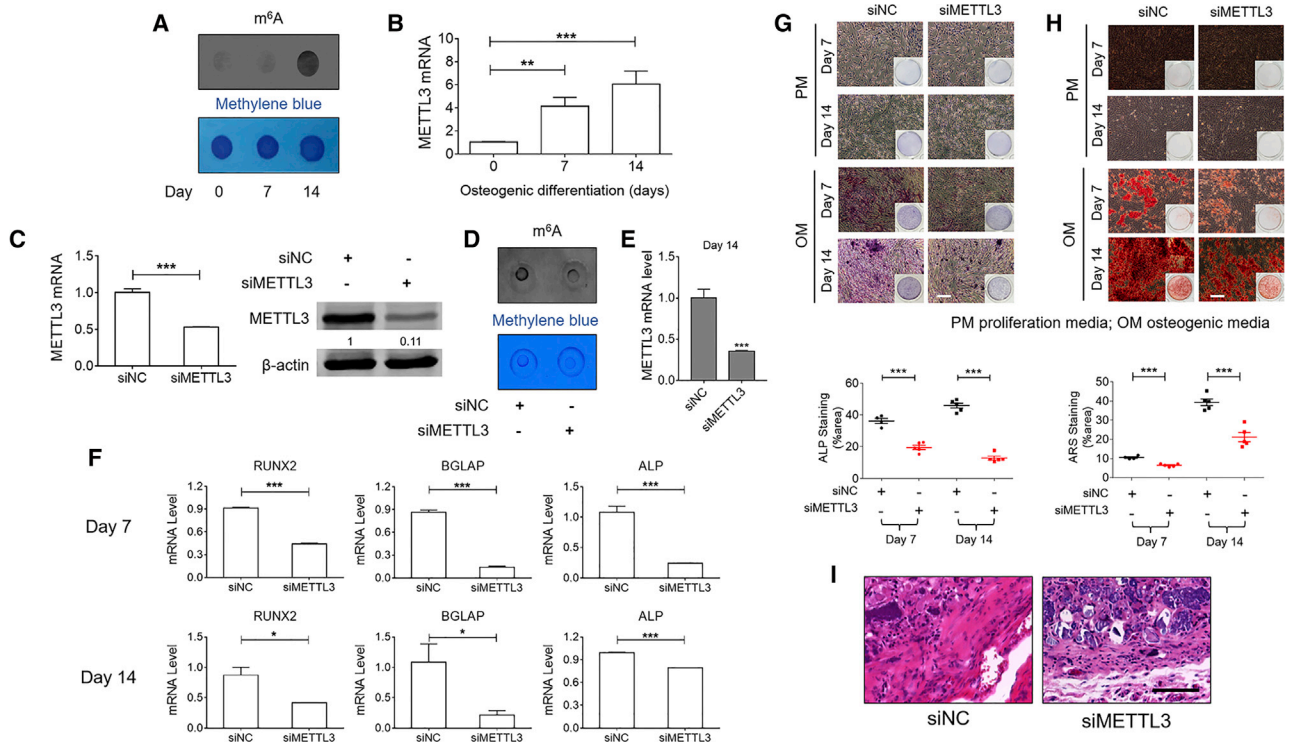

Figure 5. Silence of METTL3 Mitigates Osteogenic Differentiation of BMSCs

(A) m^{6}A dot blot analysis showing the time-dependent increase of m^{6}A content in total RNAs in BMSCs during osteogenic differentiation. n = 3. (B) qRT-PCR results showing the time-dependent upregulation of METTL3 transcripts in BMSCs 7 and 14 days after osteogenic induction. n = 8. (C) Verification of the efficiency of siMETTL3 in silencing endogenous METTL3 expression at mRNA (left panel) and protein (right panel) levels by qPCR and western blot analysis, respectively. n = 4. (D) m^{6}A dot blot assay showing the inhibitory effects of siMETTL3 on m^{6}A content in BMSCs. n = 3. (E) qRT-PCR results showing METTL3 mRNA level on day 14 after transfection with METTL3 siRNA in BMSCs, which cultured with normal complete medium. (F) The effects of METTL3 silence on the expression of key osteogenesis genes, including RUNX2, BGLAP, and ALP after 7 days (upper panels) and 14 days (lower panels) of osteogenic induction. n = 3. (G) Representative images of ALP staining (top and middle panels) showing the suppressing effect of METTL3 silencing by siMETTL3 on osteogenic differentiation of BMSCs cultured in osteogenic medium. Statistical data (bottom panel) show the decreased ALP activities by siMETTL3 relative to negative control (siRNA), as indicated by the declined percentage of the stained area. Scale bar, 150 μm, n = 6. (H) Representative images of ARS staining (top and middle panels) showing the inhibitory action of siMETTL3 on osteogenic differentiation of BMSCs cultured in osteogenic medium as indicated by diminished EMM. Statistical data (lower panel) show the increased EMM by siMETTL3 relative to siNC, as indicated by the decreased percentage of stained area. Scale bar, 150 μm, n = 6. (I) Representative H&E staining depicting the inhibitory effect of the adenovirus carrying METTL3 shRNA (siMETTL3) on bone formation of BMSCs implanted into the back of nude mice, as compared with siNC. Scale bar, 50 μm. Data are expressed as mean ± SEM. *p < 0.05; **p < 0.01; ***p < 0.001. n = 3.

showed that siMETTL3 induced bone loss in the HA/TCP particles (Figure 5I).

Identification of the METTL3/m^{6}A-pre-miR-320/miR-320-RUNX2 Axis as a Pathway Leading to Osteogenic Differentiation of BMSCs

We have demonstrated the importance of METTL3-dependent m^{6}A methylation of RNAs for osteogenic differentiation of BMSCs with both gain- and loss-of-function approaches. Next, we went on to get further insight into the molecular mechanisms that account for our findings. It has been shown that in addition to protein coding genes, large non-coding RNAs function as gene regulators during osteogenic differentiation of BMSCs.[19,20] miRNA processing is also regulated specifically for BMSCs. However, no reports have shown the biological function of m^{6}A modification during microRNA (miRNA) processing in BMSCs. To this end, we conducted the following sets of experiments.

First, we used an m^{6}A RNA immunoprecipitation (RIP) microarray to identify the target genes of METTL3 in siRNA negative control (siNC)- and siMETTL3-transfected BMSCs (Figures 6A and 6B). Of 767 pri-miRNAs and 477 precursor (pre-)miRNAs detected by the microarray, 173 pri-miRNAs and 137 pre-miRNAs were identified with significant alterations based on the threshold of >1.2-fold changes (Figure 6C). Within the genes enriched, we identified 12 pri-miRNAs with a >20% decrease (>1.2-fold decrease) in si-METTL3-treated cells relative to those in the NC cells, and 20 pre-miRNAs with a >1.2-fold decrease in their expression levels. The top 10 m^{6}A-methylated pre-miRNAs and pri-miRNAs in BMSCs are listed in Tables 1 and 2. Notably, among the pre-miRNAs,

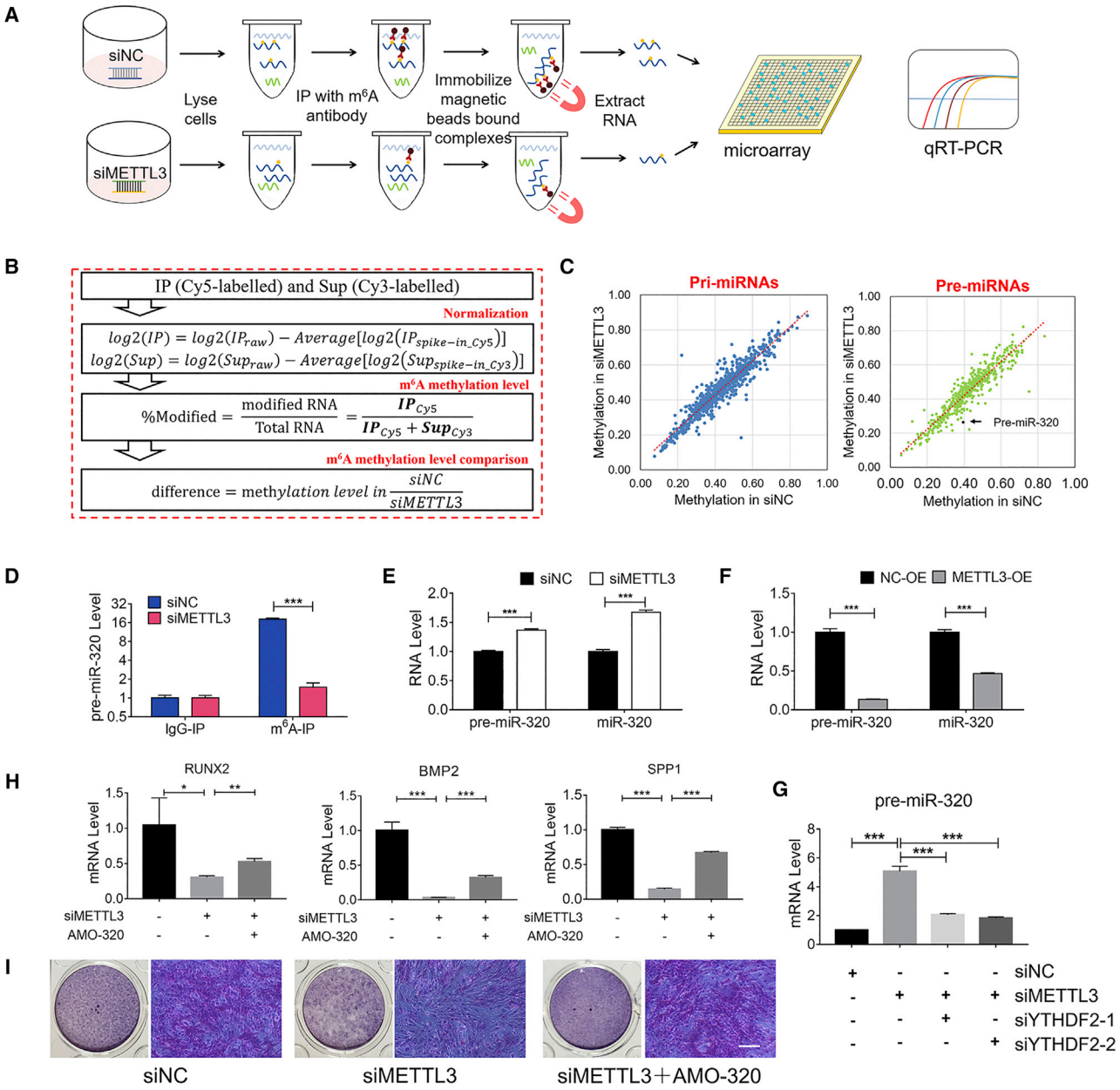

Figure 6. METTL3 Alters the m^{6}A Methylation Status of pre-miR-320 and the Expression Levels of pre-miR-320 and miR-320

(A) Flowchart showing the procedures for identifying the METTL3 targets using m^{6}A-RIP microarray analysis for RNA methylation. (B) Inhibitory effects of siMETTL3 to silence endogenous METTL3 on m^{6}A methylation of pri-miRNAs (left panel) and pre-miRNAs (right) relative to those of siNC in BMSCs. n = 3. (C) Schematic diagram showing the procedure of m6A-RIP to measure the changes of m6A enrichment in RUNX2 mRNA upon silence of METTL3 in BMSCs. (D) Inhibitory effect of siMETTL3 on pre-miRNA methylation by m^{6}A relative to that of siNC, as revealed by gene-specific m^{6}A miR-320 assay in BMSCs. n = 4. (E) Upregulation of both pre-miR-320 and miR-320 levels by siMETTL3 as determined by qRT-PCR. n = 3. (F) Downregulation of both pre-miR-320 and miR-320 levels by METTL3 overexpression (METTL3-OE). n = 3. (G) siYTHDF2 decreased expression of pre-miR-320 after co-transfection of siMETTL3. n = 3. (H) miR-320 antisense inhibitor (AMO-320) reverses the inhibitory effects of METTL3 silence on the mRNA level of key osteogenesis genes, including RUNX2, BMP2, and SPP1, after 7 days of osteogenic induction. n = 3. (I) Counteracting effect of AMO-320 to the weakening of osteogenic ability caused by siMETTL3, as indicated by ALP staining. Scale bar, 150 μm. Data are expressed as mean ± SEM. *p < 0.05, **p < 0.01, ***p < 0.001. n = 3.

Table 1. Top 10 pre-miRNAs with METTL3-Mediated m^{6}A Methylation

Gene Symbol	siNC (IP)	siMETTL3 (IP)	siNC (Supernatant)	siMETTL3 (Supernatant)	siNC (Methylation Level)	siMETTL3 (Methylation Level)	Fold Change (siMETTL3/siNC)	Conserved
pre-miR-8114	−4.77	−6.21	−4.35	−4.39	0.43	0.22	0.52	poorly
pre-miR-6974	0.42	−1.82	−1.18	−1.49	0.75	0.44	0.59	poorly
pre-miR-6994	−4.48	−5.41	−3.50	−3.54	0.34	0.21	0.64	poorly
pre-miR-320	0.53	1.17	1.14	2.65	0.40	0.26	0.67	yes
pre-miR-199a-1	−3.93	−5.21	−4.02	−4.46	0.52	0.37	0.73	yes
pre-miR-7665	−5.00	−5.37	−3.98	−3.79	0.33	0.25	0.76	poorly
pre-miR-8110	−5.31	−6.07	−3.31	−3.58	0.20	0.15	0.76	poorly
pre-miR-33	−5.31	−5.73	−4.61	−4.43	0.38	0.29	0.76	yes
pre-miR-6997	−4.63	−5.12	−4.25	−4.10	0.43	0.33	0.76	poorly
pre-miR-3073a	−2.81	−2.63	−2.01	−1.26	0.37	0.28	0.76	poorly

pre-, precursor; IP, immunoprecipitation,

pre-miR-320 is the most strongly m^{6}A methylated, and its methylation was markedly decreased upon silencing of METTL3. Moreover, pre-miR-320 sequences are highly conserved across species. These findings suggest pre-miR-320 as a potential target for METTL3 actions.

Next, we confirmed METTL3 silencing effects on m^{6}A level changes of pre-miR-320 using gene-specific m^{6}A qPCR. As shown in Figure 6D, we observed a strong enrichment of pre-miR-320 in the m^{6}A-immunoprecipitation (IP) but not in the immunoglobulin (IgG)-IP fractions; however, pre-miR-320 was much less enriched after METTL3 inhibition, indicating that pre-miR-320 was a target of METTL3 in BMSCs. In addition, inhibition of METTL3 produced significant increases in the expression levels of both pre-miR-320 and miR-320 in BMSCs (Figure 6E). On the contrary, overexpression of METTL3 produced the opposite effects (Figure 6F). Because METTL3-mediated m^{6}A methylation appeared to reduce pre-miR-320 expression, we hypothesized that pre-miR-320 is a target of YTHDF2, the m^{6}A reader protein that promotes the decay of m^{6}A methylated RNAs.[21] Consistent with our hypothesis, siRNA of YTHDF2 decreased expression of pre-miR-320 after co-transfection with knockdown of METTL3 in BMSCs (Figure 6G). Moreover, the inhibition of osteogenesis-associated genes RUNX2, BMP2, and SPP1 and the anti-osteoblast action of siMETTL3 were abrogated by co-transfection with the miR-320 inhibitor (AMO-320; Figures 6H and 6I).

To elucidate the downstream factor that likely accounts for the osteoporotic effect of the METTL3/m^{6}A-miR-320 axis or the anti-osteoporotic action of siMETTL3, we searched for the candidate target genes by computational prediction using the TargetScan miRNA database (http://www.targetscan.org/vert_72/; Figure 7A). In this way, we identified RUNX2 as a target gene for miR-320, which has also been validated by a published study.[22] RUNX2 is a key transcription factor for bone formation, with its expression upregulated during osteoblast differentiation.[23,24] Inactivation of RUNX2 exacerbates osteoporosis due to maturational arrest of osteoblast differentiation.[25] In agreement with these published findings, in the present study, RUNX2 was found to lower in its expression level in osteoporosis patients and OVX mice (Figures 7B and 7C). Overexpression of miR-320 caused a pronounced decrease in RUNX2 protein level in BMSCs as compared to NC-transfected cells (Figure 7D).

Alternatively, siMETTL3 significantly decreased the mRNA and protein levels of RUNX2 (Figures 7E and 7F). It is noteworthy that the RUNX2 gene carries 10 potential m^{6}A modification sites according to a sequence-based m^{6}A modification site predictor (http://www.cuilab.cn/sramp; Figure 7G). To clarify whether METTL3 could directly regulate the m^{6}A methylation and gene degradation of RUNX2, we performed gene-specific m^{6}A-qPCR and RNA stability assays in siNC- and siMETTL3-transfected BMSCs (Figure 7H). As expected, the m^{6}A abundance in RUNX2 mRNA was markedly decreased upon METTL3 silencing in the m^{6}A-RIP group but was not changed in the IgG-RIP group. In addition, as shown in Figure 7I, siMETTL3 reduced the stability of RUNX2 mRNA in the presence of transcription inhibitor actinomycin D (Act D) in BMSCs, whereas METTL3-OE enhanced the stability of RUNX2 mRNA. Because METTL3-mediated m^{6}A methylation promotes RUNX2 expression, we hypothesized that RUNX2 transcripts are targets of YTHDF1, the m^{6}A reader protein that promotes translation of m^{6}A methylated transcripts.[26] YTHDF1 siRNA (siYTHDF1) decreased RUNX2 protein levels in the presence of METTL3-OE to overexpress METTL3 in BMSCs (Figure 7J). Moreover, the anti-osteoblast action of siMETTL3 and the inhibition of osteogenesis-associated genes BMP2 and SPP1 were abrogated by co-transfection with overexpressed RUNX2 in BMSCs (Figures 7K and 7L).

DISCUSSION

The present study generated a number of new findings. First, METTL3 expression and m^{6}A methylation are substantially decreased in patients with osteoporosis and in a mouse model of osteoporosis induced by ovariectomy. Second, METTL3 is likely an

Table 2. Top 10 pri-miRNAs with METTL3-Mediated m^{6}A Methylation

Gene Symbol	siNC (IP)	siMETTL3 (IP)	siNC (Supernatant)	siMETTL3 (Supernatant)	siNC (Methylation Level)	siMETTL3 (Methylation Level)	Fold Change (siMETTL3/siNC)	Conserved
pri-3-miR-883b	−4.26	−7.57	−4.49	−5.41	0.54	0.18	0.34	poorly
pri-3-miR-1247	−4.20	−4.92	−3.06	−2.94	0.31	0.20	0.65	yes
pri-5-miR-6973a	−3.19	−3.52	−3.58	−2.94	0.57	0.40	0.71	poorly
pri-5-miR-30b	−4.67	−4.99	−3.44	−3.18	0.30	0.22	0.74	yes
pri-3-miR-130b	−5.08	−4.39	−5.46	−3.99	0.57	0.43	0.76	yes
pri-3-miR-3969	−4.59	−5.34	−3.89	−4.07	0.38	0.29	0.77	poorly
pri-3-miR-351	−1.85	−1.80	−1.21	−0.61	0.39	0.30	0.78	poorly
pri-3-miR-652	−5.38	−5.36	−4.44	−3.91	0.34	0.27	0.78	yes
pri-3-miR-465a	−4.43	−5.26	−3.24	−3.62	0.30	0.24	0.79	poorly
pri-3-miR-7b	−3.53	−4.16	−3.35	−3.45	0.47	0.38	0.81	poorly

pri-, primary; IP, immunoprecipitation.

anti-osteoporotic factor promoting bone formation, as its overexpression enhances osteogenic differentiation of BMSCs and its silencing produces the opposite effect. Third, m^{6}A modification of RNAs likely underlies the bone formation induced by METTL3; specifically, methylation of pre-miR-320 in nucleus by the m^{6}A mechanism causes considerable downregulation of miR-320 in cytoplasm, which may account at least partially for the osteogenic potential of METTL3. Forth, our results further demonstrated that RUNX2 is a target gene for miR-320, and METTL3/m^{6}A upregulates the RUNX2 level through suppressing pre-miR-320 and miR-320. Furthermore, we found that METTL3/m^{6}A promotes direct methylation of RUNX2 mRNA and enhances its cellular stability and thereby its cellular levels. These findings suggest that METTL3/m^{6}A fulfils the osteogenic action by upregulating cellular levels of RUNX2 through dual mechanisms: prolonging the half-life of RUNX2 by direct methylation of its mRNA, and derepressing RUNX2 by reducing miR-320 as a result of pre-miR-320 methylation. Such dual signaling cascades allowed us to draw the novel osteogenic pathways: (1) METTL3↑ → m^{6}A methylation of RUNX2↑ → RUNX2 stability/level↑ → osteogenesis↑/osteoporosis↓; and (2) METTL3↑ → m^{6}A methylation of pre-miR-320↑ → miR-320↓ → RUNX2 level↑ → osteogenesis ↑/osteoporosis↓. Our findings therefore suggest that abnormal downregulation of METTL3 is likely one of the mechanisms underlying osteoporosis in patients and mice. Under such a theme, we proposed that METTL3 is an anti-osteoporotic factor or pro-osteogenic factor, and METTL3 overexpression might be a new approach of replacement therapy for the treatment of human osteoporosis. In addition to METTL3, other components along the METTL3-m^{6}A-pre-miR-320-miR-320-RUNX2 axis could theoretically all be molecular targets for anti-osteoporotic therapy.

It is known that RUNX2, localized within both the nucleus and cytosol, is an early and key osteogenesis-related gene.[27] Several studies have demonstrated that osteogenesis is controlled by multiple cellular factors and modulated by some therapeutic agents. For instance, resveratrol favors osteogenesis of human MSCs by upregulating RUNX2 via the SIRT1-FOXO3A axis.[28] miR-21 promotes osteogenesis of BMSCs by enhancing the Smad7-Smad1/5/8-RUNX2 signaling pathway.[29] VEGF controls differentiation of MSCs by regulating RUNX2 and PPARγ2 as well as through a reciprocal interaction with nuclear envelope proteins lamin A/C.[30] However, before the present study, it was unclear whether RNA methylation takes place on RUNX2, a critical pro-osteogenic or anti-osteoporotic gene. In this study, we for the first time unraveled that METTL3 could directly induce m^{6}A methylation of RUNX2 mRNA to enhance its cellular stability and indirectly upregulate the cellular level of RUNX2 via m^{6}A methylation of pre-miR-320. More importantly, our data indicate that such dual mechanisms can ensure a higher level and longer half-life of RUNX2, and abnormal downregulation of METTL3 contributes significantly to the development of osteoporosis, presumably owing to a withdrawal of the dual mechanisms of action of METTL3.

A pre-miRNA is generally exported by Exportin-5 from the nucleus to the cytoplasm where its loop structure of hairpin is further cleaved by the RNase III enzyme Dicer to generate mature a miRNA.[31] Once a mature miRNA is incorporated into the RNA-induced silencing complex (RISC), the expression of its targeted genes is repressed. Several studies have revealed the roles of miRNAs in osteogenic differentiation and bone formation. For instance, overexpression of miR-335-5p driven by an osterix promoter induces osteogenic differentiation and bone formation in mice.[32] miR-205 is downregulated in a time-dependent manner during the osteoinduction of BMSCs, and this downregulation enhances osteogenic potential partly via altering phosphorylation of extracellular signal-regulated kinase (ERK) and p38 mitogen-activated protein kinase (MAPK).[33] Our m^{6}A-RIP microarray data demonstrated that pre-miR-320 was enriched in an m^{6}A-RIP fraction with METTL3 overexpression, which retarded the osteogenic differentiation of BMSCs and bone formation. This favorable and desirable action of METTL3 was mitigated by silencing METTL3. An intriguing new finding here is that pre-miRNAs can be methylated in the nucleus, leading to reduced biogenesis of mature miRNAs. Yet, it remains unknown how exactly the methylation of

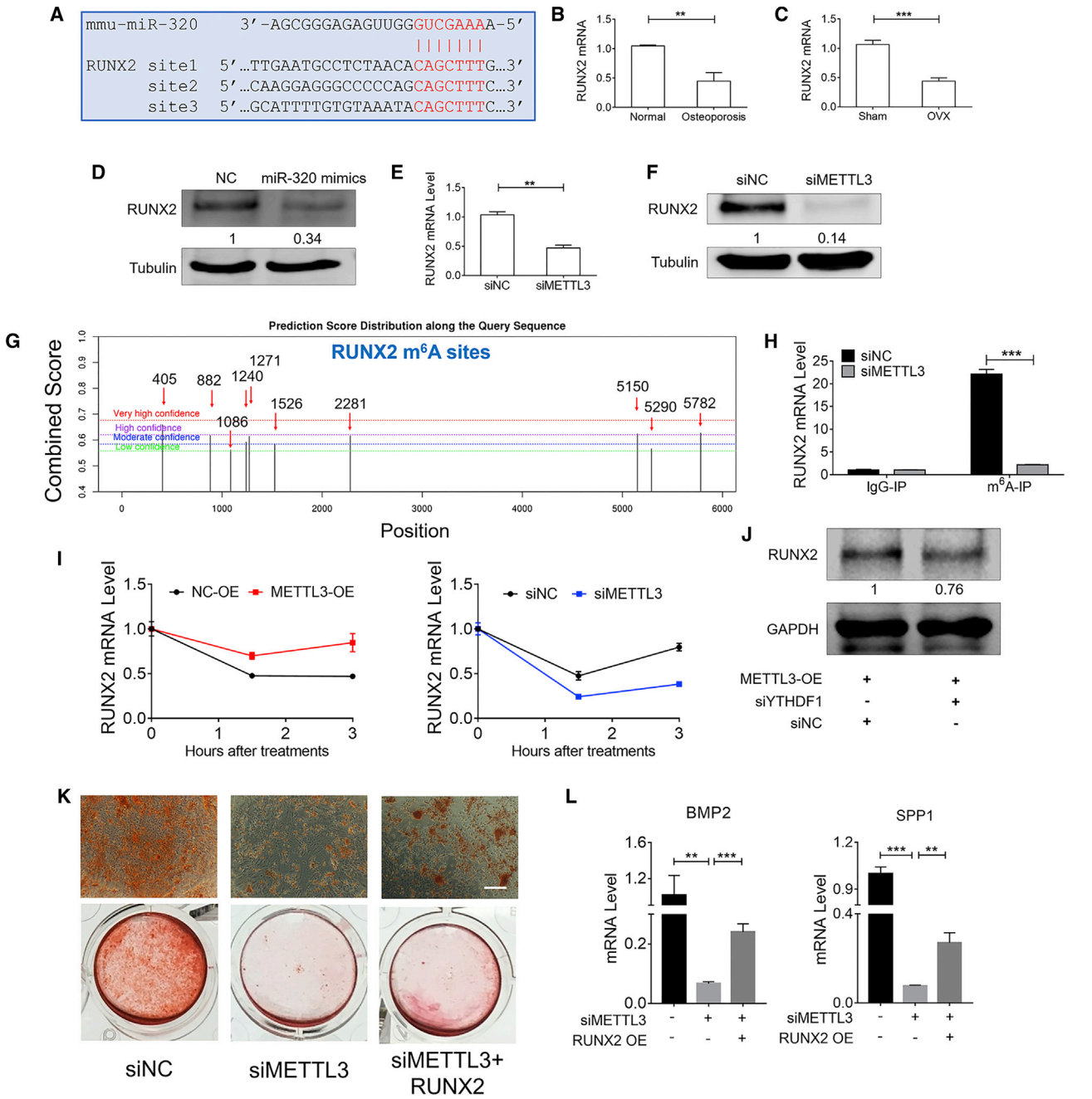

Figure 7. RUNX2 as a Target Gene of miR-320 and a Mediator of the Osteogenic Action of the METTL3/m^{6}A Modification Axis

(A) Sequence alignment showing the complementarity between miR-320 and RUNX2 gene with three potential binding sites (seed sites). The bases in red indicate the seed site, and the vertical lines represent the base pairing between miR-320 and RUNX2. (B and C) Lower expression levels of RUNX2 in bone tissues in osteoporosis patients than in healthy subjects (B; n = 6) and in OVX mice than in sham-control counterparts (C; n = 7). (D) Western blot results showing the repressive effect of miR-320 on RUNX2 protein level in BMSCs. n = 3. (E and F) Downregulation of RUNX2 at both mRNA (E) and protein (F) levels by silencing METTL3 with siMETTL3, as reported by qRT-PCR and western blot analysis. n = 3. (G) Potential sites and regions for m^{6}A modification in the sequence of RUNX2 gene. (H) Gene-specific m^{6}A-qPCR assay showing the reduction of m^{6}A modification in specific regions of RUNX2 gene by siMETTL3 in BMSCs. (I) Changes of half-life ($t_{1/2}$) of RUNX2 mRNA in BMSCs with or without METTL3 depletion. (J) YTHDF1 siRNA (siYTHDF1) downregulates RUNX2 expression in the presence of METTL3-OE. (K) Alizarin red S staining results showing a slight recovery to osteogenic ability weakened by siMETTL3 in BMSCs. Scale bar, 150 μm. (L) RUNX2 overexpression exhibited a reversion effect on mRNA levels of BMP2 and SPP1, which was decreased by siMETTL3 after 7 days of osteogenic induction. n = 3. Data are expressed as mean ± SEM. **p < 0.01, ***p < 0.001.

pre-miR-320 in the nucleus affects its maturation in the cytosol. This issue merits future studies. Moreover, in this study we only observed rescue phenotypes of METTL3 depletion by overexpression of RUNX2 or knockout of miR-320 *in vitro*. It will certainly be interesting to confirm the mechanisms in an *in vivo* study.

The most common therapies for osteoporosis were inhibition of bone resorption and stimulation of formation by using calcitonin, vitamin D derivatives, bisphosphonates, estrogens, selective estrogen receptor modulators, and parathyroid hormone (PTH).[34,35] Recent preclinical studies and clinical trials have demonstrated the promising application of stem cell therapies for the treatment of osteoporosis.[10,36,37] It has been documented that in patients with osteoporosis, BMSCs undergo unfavorable changes with weakened potential to differentiate into osteoblasts and an enhanced capability and trend to transform into adipocytes.[38] Because of this issue, tremendous research efforts have been reorient to the balance between osteoblast and adipocyte differentiation of BMSCs. Consistent with our findings, Wu et al.[39] indeed showed that overexpression of METTL3 prevents estrogen deficiency-induced osteoporosis. They also identified the Pth1r signaling axis as an important METTL3-mediated m^{6}A downstream mechanism pathway. However, in our study, we found that METTL3-mediated m^{6}A methylation of pre-miR-320 promotes the osteogenic differentiation process of BMSCs and bone formation. Strikingly, miRNAs have been reported to play essential roles in the fine regulation of the balance. For instance, miR-188 reduces bone formation and simultaneously increases bone marrow fat accumulation.[40] Overexpression of miR-23a/b promotes osteogenic differentiation, whereas knockdown of miR-23a/b increases adipogenic differentiation in BMSCs.[41] We further elucidated that the downstream mechanisms for the effects of pre-miR-320 methylation could be ascribed to reduced biogenesis of mature miR-320 and thereby increased RUNX2 expression due to derepression from basal miR-320 activities. As we showed in the m^{6}A-RIP microarray data above, we identified 12 pri-miRNAs and 20 pre-miRNAs with a >20% decrease in si-METTL3-treated cells versus in the NC cells. Actually, we identified even more pri-miRNAs and pre-miRNAs (49 pri-miRNAs and 21 pre-miRNAs) that had increased expression levels in siMETTL3-treated cells. As is known, m^{6}A methyltransferases have recently emerged as key regulators of gene expression, except METTL3. For example, METTL16 is an active m^{6}A methyltransferase also by targeting pre-mRNAs and various non-coding RNAs.[42] Therefore, the METTL3 knockout/inhibition might result in some genes with more sensitivity to those of other m^{6}A methyltransferases. Alternatively, these increased pri-miRNAs and pre-miRNAs might also be caused by experimental set-up and normalization procedures. Strong decreased effects of one or more genes might lead to false increased effects and vice versa. However, these increased pri-miRNAs and pre-miRNAs might also be interesting candidates in further studies.

An intriguing point revealed by the present study is that METTL3-meidtaed m^{6}A methylation of different genes could lead to different outcomes: downregulation of pre-miR-320 level and upregulation of RUNX2 level upon methylation by m^{6}A. In other words, silencing METTL3 abrogated m^{6}A methylation and resulted in upregulation of pre-miR-320 and downregulation of RUNX2. Such gene-specific effects of methylation or differential outcomes of methylation (enhancing and depressing the final levels of targeted genes of different kinds) should bear some important implications in the differentiation lineages and pathophysiological roles. However, we must admit that the underlying mechanisms are at present unknown.

Collectively, our results suggest that METTL3 is an anti-osteoporotic factor or a pro-osteogenic factor, acting at least partially by maintaining RUNX2 expression at a higher level through dual mechanisms with direct m^{6}A methylation of RUNX2 and indirect upregulation of RUNX2 level due to methylation of pre-miR-320. We have also demonstrated that pre-miRNAs could be methylated by the METTL3/m^{6}A mechanism in the nucleus, leading to significant alterations of their maturation in the cytosol. Moreover, the outcomes (e.g., the cellular levels) of RNAs subjected to m^{6}A methylation appear to be gene specific, with some exhibiting positive and others negative changes of their cellular levels. In addition, METTL3 might be considered a molecular target for the development of new strategies for the treatment of osteoporosis owing to the highly desirable property of METTL3 replacement in favoring osteogenic differentiation of BMSCs and bone formation.

MATERIALS AND METHODS

Human Bone Samples

Bone samples were obtained from three patients with osteoporosis (female) at ages ranging from 54 to 65 years, as well as from three female control subjects without osteoporosis and other bone-related anomalies (18–25 years old). The sample collection was conducted by the Department of Orthopedics, The First Affiliated Hospital of Harbin Medical University. The experimental protocols were approved by the Experimental Animal Ethics Committee of Harbin Medical University.

Generation and Maintenance of METTL3$^{+/-}$ Mice

METTL3$^{+/-}$ mice (C57BL/6J background) were purchased from Cyagen (Guangzhou, Guangdong, China). Briefly, an METTL3 targeting construct was linearized by restriction digestion with NotI, followed by phenol/chloroform extraction and ethanol precipitation. The linearized vector was transfected into C57BL/6 embryonic stem cells (ESCs) according to the manufacturer's standard electroporation procedures. The transfected ESCs were subjected to G418 selection (200 μg/mL) 24 h after electroporation. G418-resistant clones were picked and amplified in 96-well plates. Two copies of 96-well plates were prepared with one frozen and stored at −80°C and the other used for DNA isolation and subsequent PCR screening for homologous recombination. The PCR screening identified six potential targeted clones, each of which was expanded and characterized by Southern blot analysis. All six expanded clones were confirmed to be correctly targeted.

Eight-week-old C57BL/6 mice were purchased from The Second Affiliated Hospital of Harbin Medical University. Female immunocompromised nude mice (BALB/c, nu/nu) were purchased from

Charles River (Beijing Vital River Laboratory Animal Technology, Beijing, China). The animals were maintained under pathogen-free conditions in the animal facility in Harbin Medical University, and the animal experimental protocol was approved by the Institutional Animal Care and Use Committee of Harbin Medical University.

Mouse Model of Osteoporosis

Experiments were performed following the Guidelines of the Institutional Animal Use and Care Committee of Harbin Medical University. Eight-week-old female C57BL/6 mice were selected for ovariectomy and randomly assigned to the sham-controlled group (the bilateral ovaries were exposed and nearby adipose tissue was removed) or the OVX group (the bilateral ovaries were removed) with n = 5 per group. Ovaries were surgically removed on both sides after anesthesia. A 50-mm incision was made in the back of the mouse, and the muscle tissue was carefully peeled off to expose the ovaries. The ovaries were removed after ligation of the fallopian tubes. Finally, the wound was sutured, and the mice were bred for another 8 weeks before they were sacrificed.

RNA Extraction

Total RNA was isolated using the miRNeasy Mini kit (QIAGEN) according to the manufacturer's protocol. Briefly, cells were disrupted and homogenized with QIAzol lysis reagent at room temperature (RT) for 5 min. Then, chloroform was added to the samples followed by vigorous shaking for 15 s. After centrifugation at 12,000 × *g* at 4°C for 15 min, the upper aqueous phase was transferred to a new collection tube and mixed with ethanol thoroughly. The sample of 700 μL was pipetted into an RNeasy Mini column followed by centrifugation at 8,000 × *g* at RT for 15 s to discard the flow-through. After washing sequentially with RWT buffer and then RPE buffer, RNAs were dissolved in RNase-free water.

m^{6}A Dot Blot

An m^{6}A dot blot was used to detect total m^{6}A levels in RNA samples. RNAs were directly spotted onto a Hybond-N+ membrane (catalog #RPN303B; Biosharp, Guangzhou, China) and then UV-crosslinked to the membrane using a Stratalinker 2400 UV crosslinker (catalog #CL-1000; UVP, Upland, CA, USA). After washing with Tris-buffered saline with Tween 20 (TBST) for 5 min to remove unbound mRNAs, the membrane was blocked with 5% non-fat dry milk at RT for 1 h and incubated with anti-m^{6}A antibody (1:500 dilution; catalog #202003; Synaptic Systems, Germany) at 4°C overnight. After washing with TBST three times, the membrane was incubated with the horseradish peroxidase (HRP)-conjugated goat anti-rabbit IgG (1:500 dilution; catalog #202003; Synaptic Systems) at RT for 1 h. Finally, the membrane was analyzed with Odyssey version 1.2 software (LI-COR Biosciences, Lincoln, NE, USA).

m^{6}A Quantification

Quantification of m^{6}A RNA methylation was detected by an m^{6}A RNA methylation assay kit (catalog #ab185912; Abcam, Cambridge, UK) following the manufacture's protocol. Total RNA samples of 200 ng for each group were used to determine the percentage of m^{6}A. The absorbance was measured at 450 nm using a microplate reader, and the percentage of m^{6}A in total RNA was calculated using the following equation:

$$m^6A\% = \frac{(\text{Sample}_{OD} - \text{NC}_{OD}) \div S}{(\text{PC}_{OD} - \text{NC}_{OD}) \div P} \times 100\%,$$

where S represents the amount of input RNA sample (ng), P is the amount of input of positive control (ng), and PC represents the positive control.

Adenovirus Injection

METTL3-carrying adenovirus for overexpression (METTL3-OE) and empty vector-carrying adenovirus (NC-OE) were constructed by Cyagen (Guangzhou, China). Six 8-week-old female mice were randomly selected to receive adenovirus treatment. METTL3-carrying adenovirus of 20 μL (the titer is 1×10^{10} plaque-forming units [PFU]/mL) or NC-OE of an equal volume was intramuscularly injected vertically into the lateral thigh muscle of the mice every 2 days for three consecutive injections. The bone tissue RNAs were extracted on day 7 after injection for verifying the infection efficiency. Then, the mice were subjected to ovariectomy to create the osteoporosis model. Eight weeks after ovariectomy, the femur was dissected for the mice for subsequent experimental studies.

Bone μ-CT Analysis

The femurs were fixed with 4% paraformaldehyde (PFA) at 4°C for 48 h and then decalcified for 3 weeks before scanning and analysis. The gross bone morphology and microarchitecture were analyzed with a Skyscan1076 instrument (SkyScan, Belgium).

BMSC Culturing

BMSCs from C57BL/6 mice (MUBMX-01001) were purchased from Cyagen (Guangzhou, China) and cultured in BMSC complete medium (MUBMX-90011; Cyagen) at 37°C in a humidified environment containing 5% CO_2. Experiments were performed with BMSCs of $\leq$10 passages.

siRNA Transfection

siRNA of 15 nM was transfected into BMSCs using Lipofectamine RNA iMAX reagent (MAN0007825; Invitrogen, Carlsbad, CA, USA) according to the manufacturer's instructions to silence gene expression. Subsequent experimental measurements were performed 24 h after transfection. The sequences of siRNAs used are METTL3: sense, 5′-GCUGCACUUCAGACGAAUUTT-3′, antisense, 5′-AAUUCGUCUGAAGUGCAGCTT-3′; YTHDF2 siRNA-1: sense, 5′-GGAAGAAGAAAGUGUUAAATT-3′, antisense, 5′-UUUAACACUUUCUUCUUCCTT-3′; and YTHDF2, siRNA-2, sense, 5′-ACUCAAAGCUCUGGAUAUATT-3′, antisense, 5′-UAUAUCCAGAGCUUUGAGUTT-3′.

Plasmid Transfection

METTL3-carrying plasmid for overexpression in BMSCs and NC plasmid were constructed by Cyagen. BMSCs were transfected with 1 μg of METTL3 plasmid using X-tremeGENE HP DNA transfection

Table 3. The Primer Sequences Used for Quantitative Real-Time PCR

Primer	Forward Primer (5′→3′)	Reverse Primer (5′→3′)
h-METTL3 (NM_019852.5)	CGACGGAAGTATCGCTTGTCA	TTCACCGAGGTCAGCAGTATG
h-METTL14 (NM_020961.4)	GTCTTAGTCTTCCCAGGATTGTTT	AATTGATGAGATTGCAGCACC
h-FTO (XM_011523316.3)	GACCTGTCCACCAGATTTTCA	AGCAGAGCAGCATACAACGTA
h-ALKBH5 (NM_017758.4)	ACTGAGCACAGTCACGCTTCC	GCCGTCATCAACGACTACCAG
h-RUNX2 (NM_001024630.4)	CCACTGAACCAAAAAGAAATCCC	GAAAACAACACATAGCCAAACGC
h-BGLAP (NM_199173.6)	CTCACACTCCTCGCCCTATTGG	GTAGCGCCTGGGTCTCTTCACT
h-BMP2 (NM_001200.4)	GGGAGAAGGAGGAGGCAAACAA	CTGGGGAAGCAGCAACGCTA
h-Col1a1 (NM_000088.4)	CGATGGATTCCAGTTCGAGTATG	TGTTCTTGCAGTGGTAGGTGATG
h-GAPDH (NM_001256799.3)	CATGTTCGTCATGGGTGTGAA	GGCATGGACTGTGGTCATGAG
m-METTL3 (NM_019721.2)	CTTTCTACCCCATCTTGAGTG	CCAACCTTCCGTAGTGATAGTC
m-METTL14 (NM_201638.2)	TCTGGAAAACTGCCTTTGGAT	AAATGCTGGACCTGGGATGAT
m-FTO (NM_011936.2)	GACTCGTCCTCACTTTCATCC	AAGAGCAGAGCAGCCTACAAC
m-ALKBH5 (NM_172943.4)	GTGGGACCTTTTGGGTTTCAG	GCATACGGCCTCAGGACATTA
m-RUNX2 (NM_001145920.2)	ACTTCCTGTGCTCCGTGCTG	TCGTTGAACCTGGCTACTTGG
m-BGLAP (NM_007541.3)	CTCTGTCTCTCTGACCTCACAG	CAGGTCCTAAATAGTGATACC
m-BMP2 (NM_007553.3)	CCTTGCTGACCACCTGAACT	AACATGGAGATTGCGCTGA
m-Osterix (NM_001348205.1)	ACCAGGTCCAGGCAACAC	GCAAAGTCAGATGGGTAAGTAG
m-ALP (NM_001287172.1)	GCCTGGATCTCATCAGTATTTGG	GTTCAGTGCGGTTCCAGACAT
m-GAPDH (NM_008084.3)	ACCACAGTCCATGCCATCAC	TCCACCACCCTGTTGCTGTA

h-, human; m-, mouse.

reagent (catalog #26540900; Roche, Basel, Switzerland) according to the manufacturer's protocols. Cells were collected 24 h after transfection.

Measurement of Osteogenic Differentiation

Osteogenic medium (MUBMX-90021; Cyagen) was used according to the manufacturer's protocol to induce differentiation of BMSCs into osteoblasts. Briefly, BMSCs were inoculated onto a six-well plate coated with gelatin (GLT-11301; Cyagen) at a cell density of 2×10^4 cells/cm^2. When the cell confluence reached 60%–70%, 2 mL of osteogenic differentiation medium was carefully added to the plate. The fresh induction medium was replaced every 3 days.

ARS Staining

ARS staining was used to evaluate calcium-rich deposits in cultured cells. On days 7 and 14 of osteogenic differentiation, BMSCs were fixed with 4% formaldehyde at RT for 30 min and washed with PBS three times. Next, the cells were stained with 40 mM ARS solution (S0141; Cyagen) at RT for 5 min. The images of the stained cells were scanned by light microscopy (Eclipse TS100; Nikon, Melville, NY, USA). The alizarin red-positive area indicating osteogenesis was calculated using ImageJ software (National Institutes of Health [NIH], USA).

ALP Assay

An ALP assay was used to evaluate the phenotype of osteoblast differentiation of BMSCs using an ALP kit (SLBV5860; Sigma-Aldrich, St. Louis, MO, USA). Briefly, BMSCs were fixed with 4% PFA (m/v) for 30 min after discarding medium and washing with deionized water. Sodium nitrite solution (22.2 μL) and fast red violet (FRV)-alkaline solution (22.2 μL) were mixed at RT for 2 min and the mixed solution was added to 1 mL of deionized water pre-warmed to 25°C. Next, 22.2 μL of AS-BI alkaline solution was added to 1 mL of deionized water to dilute diazonium salt solution. Cells were incubated in the dark at RT for 15 min. The cells were washed with deionized water twice and then counterstained with staining solution for 2 min. Finally, images were taken using standard light microscopy (Eclipse TS100; Nikon).

Quantitative Real-Time PCR

Total RNA sample of 500 ng was reverse transcribed to cDNA using a high-capacity cDNA reverse transcription kit (catalog #00676299; Thermo Fisher Scientific, Waltham, MA, USA). Amplification and detection were performed using a 7500HT Fast real-time PCR system (Applied Biosystems, Waltham, MA, USA) with SYBR Green PCR master mix (catalog #31598800; Roche). GAPDH was used as endogenous control. Reactions were run in triplicate. The sequences of primers used for quantitative real-time PCR amplification are listed in Table 3.

H&E Staining

H&E staining of mouse femurs was used to detect bone formation ability in mice. Femurs were dissected out from mice after euthanasia, and the surrounding muscle tissues were removed. Subsequently, the femurs were fixed in 4% PFA (m/v) for 24 h, decalcified in 10% EDTA

for 20 days, and embedded in paraffin. Bone sections were stained with H&E (catalog #C0105; Beyotime Biotechnology) to quantify the number and surface area of osteoblasts and adipocytes.

Western Blot Analysis

BMSCs were lysed in cell lysis buffer (catalog #P0013B; Beyotime Biotechnology, Shanghai, China) supplemented with PMSF protease inhibitor on ice for 30 min, followed by centrifugation at 13,500 × *g* at 4°C for 15 min. The protein concentration was quantified using a bicinchoninic acid (BCA) protein assay kit (catalog #P0010S; Beyotime Biotechnology) following the manufacturer's instructions. Protein samples (50 μg) were separated on polyacrylamide gel, transferred onto a nitrocellulose membrane, and then blocked with 5% fat-free dry milk at RT for 1 h. Next, the membrane was incubated with rabbit anti-RUNX2 antibody (1:1,000; catalog #8486; Cell Signaling Technology, Danvers, MA, USA), rabbit anti-METTL3 antibody (1:1,000; catalog #A8370; ABclonal, Woburn, MA, USA), mouse anti-tubulin antibody (1:1,000; catalog #abs830032; Absin, Shanghai, China), or mouse anti-β-actin antibody (1:1,000, catalog #sc-47778; Santa Cruz Biotechnology) at 4°C overnight. A secondary incubation step was carried out with monoclonal anti-rabbit IgG (1:5,000, catalog #14708; Abcam) or monoclonal anti-mouse IgG (1:5,000, catalog #3420; Abcam) at RT for 1 h. Western blot bands were imaged by Odyssey CLx and quantified with LI-COR Image Studio software (LI-COR Biosciences, Lincoln, NE, USA).

BMSC-Mediated Bone Formation *In Vivo*

BMSCs were transfected according to the procedures described above. Briefly, approximately 1×10^6 cells were mixed with hydroxyapatite/tricalcium phosphate (HA/TCP) ceramic particles (40 mg; Zimmer, Warsaw, IN, USA) as a carrier and incubated at 37°C overnight. The cells were then subcutaneously implanted in 8-week-old immunocompromised mice. Eight weeks post-implantation, the mice were euthanized, and the implants were harvested and fixed with 4% PFA at 4°C for 48 h and then embedded in paraffin. Six-micrometer-thick sections were stained with H&E.

Microarray Analysis

Total RNA samples were extracted from METTL3-silenced BMSCs and the corresponding non-target control cells. The samples were incubated with m^6A antibody for IP. The modified RNAs were eluted from the immunoprecipitated magnetic beads as the "IP," and the unmodified RNAs were recovered from the supernatant as "Sup." The RNAs were labeled with Cy5 and Cy3, respectively, and designated as cRNAs in separate reactions using the Arraystar Super RNA labeling kit (Arraystar, Rockville, MD, USA). The cRNAs were combined together and hybridized onto the Arraystar Mouse Epitranscriptomic Microarray (8 × 60K, Arraystar). After washing the slides, the arrays were scanned in two-color channels by an Agilent G2505C scanner. Raw intensities of IP (Cy5-labeled) and Sup (Cy3-labeled) were normalized with the average of log_2-scaled spike-in RNA intensities. After spike-in normalization, the probe signals having present (P) or marginal (M) quality control (QC) flags in at least one out of two samples were retained as "all targets value" in the Excel sheet for determination of m^6A methylation level and m^6A quantity. The m^6A methylation level was calculated as the percentage of modification based on the IP (Cy5-labeled) and Sup (Cy3-labeled) normalized intensities. m^6A quantity was calculated to indicate the degree of m^6A methylation of RNAs based on the IP normalized intensities. Differentially m^6A-methylated RNAs were identified by filtering with fold changes of >1.2.

Methylated RIP-qPCR

The Magna methylated RIP (MeRIP) kit (Millipore, cat. #CR203146) was used to examine m^6A modification of genes according to the manufacturer's instructions. Cells were harvested prior to washing with ice-cold PBS twice, and subsequently collected by centrifugation at 1,500 rpm at 4°C for 5 min. After removal of the supernatant, the cells were mixed with 100 μL of RIP lysis buffer and incubated with the lysate on ice for 5 min. The cell preparation was then stored at −80°C. m^6A antibody (5 μg) was added to a tube containing magnetic beads, followed by rotation at RT for 30 min. The beads were washed with RIP wash buffer twice and resuspended in 900 μL of RIP buffer mixed with 100 μL of cell lysate followed by centrifugation at 14,000 rpm at 4°C for 10 min. After rotation at 4°C overnight, the beads were washed with high-salt buffer, followed by extraction of RNAs with RIP wash buffer. The RNA enrichment was analyzed by qRT-PCR.

RNA Stability Assay

Cells were plated onto six-well plates and transfected with desired constructs as described above. After 24 h of transfection, cells were treated with actinomycin D (5 μg/mL; catalog #HY-17559; Sigma) for 0, 1.5, and 3 h before collection. Total RNAs were isolated for qRT-PCR analysis.

Statistical Analysis

Data are expressed as mean ± SEM. Statistical analysis was performed with one-way analysis of variance (ANOVA) for multiple group comparisons and Student's t test (two-tailed) for two-group comparisons (GraphPad, San Diego, CA, USA). All experiments were independently repeated at least three times. A p value <0.05 was considered statistically significant (*$p < 0.05$, **$p < 0.01$, ***$p < 0.001$).

SUPPLEMENTAL INFORMATION

Supplemental Information can be found online at https://doi.org/10.1016/j.omtn.2019.12.001.

AUTHOR CONTRIBUTIONS

G.Y., M.H., R.G., H.L., H.Z., W.W., T.M., S.L., Z.X., M.G., and M.Y. performed research; Y.Y., G.Y., M.H., W.D., Y.B., P.P., X.L., S.Y., and F.Y. analyzed data; and Y.Y., B.C., and L.Y. designed the study and wrote the manuscript.

CONFLICTS OF INTEREST

The authors declare no competing interests.

ACKNOWLEDGMENTS

This work was supported by grants from the National Natural Science Foundation of China (81972117, 81501920, and 81800784), the Natural Science Foundation of Heilongjiang Province (H2015056), the Postdoctoral Scientific Research Developmental Fund of Heilongjiang Province (LBH-Q18084), and the Wuliande Foundation of Harbin Medical University (WLD-QN1712).

REFERENCES

1. Cao, G., Li, H.B., Yin, Z., and Flavell, R.A. (2016). Recent advances in dynamic m6A RNA modification. Open Biol. *6*, 160003.
2. Yue, Y., Liu, J., and He, C. (2015). RNA N^6-methyladenosine methylation in post-transcriptional gene expression regulation. Genes Dev. *29*, 1343–1355.
3. Desrosiers, R., Friderici, K., and Rottman, F. (1974). Identification of methylated nucleosides in messenger RNA from Novikoff hepatoma cells. Proc. Natl. Acad. Sci. USA *71*, 3971–3975.
4. Yang, Y., Hsu, P.J., Chen, Y.S., and Yang, Y.G. (2018). Dynamic transcriptomic m^6A decoration: writers, erasers, readers and functions in RNA metabolism. Cell Res. *28*, 616–624.
5. Ping, X.L., Sun, B.F., Wang, L., Xiao, W., Yang, X., Wang, W.J., Adhikari, S., Shi, Y., Lv, Y., Chen, Y.S., et al. (2014). Mammalian WTAP is a regulatory subunit of the RNA N^6-methyladenosine methyltransferase. Cell Res. *24*, 177–189.
6. Pan, Y., Ma, P., Liu, Y., Li, W., and Shu, Y. (2018). Multiple functions of m^6A RNA methylation in cancer. J. Hematol. Oncol. *11*, 48.
7. Li, Z., Weng, H., Su, R., Weng, X., Zuo, Z., Li, C., Huang, H., Nachtergaele, S., Dong, L., Hu, C., et al. (2017). FTO plays an oncogenic role in acute myeloid leukemia as a N^6-methyladenosine RNA demethylase. Cancer Cell *31*, 127–141.
8. Mathiyalagan, P., Adamiak, M., Mayourian, J., Sassi, Y., Liang, Y., Agarwal, N., Jha, D., Zhang, S., Kohlbrenner, E., Chepurko, E., et al. (2019). FTO-dependent N^6-methyladenosine regulates cardiac function during remodeling and repair. Circulation *139*, 518–532.
9. Ma, J.Z., Yang, F., Zhou, C.C., Liu, F., Yuan, J.H., Wang, F., Wang, T.T., Xu, Q.G., Zhou, W.P., and Sun, S.H. (2017). METTL14 suppresses the metastatic potential of hepatocellular carcinoma by modulating N^6-methyladenosine-dependent primary microRNA processing. Hepatology *65*, 529–543.
10. Antebi, B., Pelled, G., and Gazit, D. (2014). Stem cell therapy for osteoporosis. Curr. Osteoporos. Rep. *12*, 41–47.
11. Poon, Z., Dighe, N., Venkatesan, S.S., Cheung, A.M.S., Fan, X., Bari, S., Hota, M., Ghosh, S., and Hwang, W.Y.K. (2019). Bone marrow MSCs in MDS: contribution towards dysfunctional hematopoiesis and potential targets for disease response to hypomethylating therapy. Leukemia *33*, 1487–1500.
12. Tompkins, B.A., Balkan, W., Winkler, J., Gyöngyösi, M., Goliasch, G., Fernández-Avilés, F., and Hare, J.M. (2018). Preclinical studies of stem cell therapy for heart disease. Circ. Res. *122*, 1006–1020.
13. Yang, F., Yang, L., Li, Y., Yan, G., Feng, C., Liu, T., Gong, R., Yuan, Y., Wang, N., Idiiatullina, E., et al. (2017). Melatonin protects bone marrow mesenchymal stem cells against iron overload-induced aberrant differentiation and senescence. J. Pineal Res. *63*, e122422.
14. Kim, J., and Ko, J. (2014). A novel PPARγ2 modulator sLZIP controls the balance between adipogenesis and osteogenesis during mesenchymal stem cell differentiation. Cell Death Differ. *21*, 1642–1655.
15. Liao, L., Yang, X., Su, X., Hu, C., Zhu, X., Yang, N., Chen, X., Shi, S., Shi, S., and Jin, Y. (2013). Redundant miR-3077-5p and miR-705 mediate the shift of mesenchymal stem cell lineage commitment to adipocyte in osteoporosis bone marrow. Cell Death Dis. *4*, e600.
16. NIH Consensus Development Panel on Osteoporosis Prevention, Diagnosis, and Therapy (2001). Osteoporosis prevention, diagnosis, and therapy. JAMA *285*, 785–795.
17. Bianco, P., Robey, P.G., and Simmons, P.J. (2008). Mesenchymal stem cells: revisiting history, concepts, and assays. Cell Stem Cell *2*, 313–319.
18. Chen, X., Zhi, X., Wang, J., and Su, J. (2018). RANKL signaling in bone marrow mesenchymal stem cells negatively regulates osteoblastic bone formation. Bone Res. *6*, 34.
19. Yang, L., Li, Y., Gong, R., Gao, M., Feng, C., Liu, T., Sun, Y., Jin, M., Wang, D., Yuan, Y., et al. (2019). The long non-coding RNA-ORLNC1 regulates bone mass by directing mesenchymal stem cell fate. Mol. Ther. *27*, 394–410.
20. Yang, D., Qiao, J., Wang, G., Lan, Y., Li, G., Guo, X., Xi, J., Ye, D., Zhu, S., Chen, W., et al. (2018). N^6-methyladenosine modification of lincRNA 1281 is critically required for mESC differentiation potential. Nucleic Acids Res. *46*, 3906–3920.
21. Wang, X., Lu, Z., Gomez, A., Hon, G.C., Yue, Y., Han, D., Fu, Y., Parisien, M., Dai, Q., Jia, G., et al. (2014). N^6-methyladenosine-dependent regulation of messenger RNA stability. Nature *505*, 117–120.
22. Hamam, D., Ali, D., Vishnubalaji, R., Hamam, R., Al-Nbaheen, M., Chen, L., Kassem, M., Aldahmash, A., and Alajez, N.M. (2014). MicroRNA-320/RUNX2 axis regulates adipocytic differentiation of human mesenchymal (skeletal) stem cells. Cell Death Dis. *5*, e1499.
23. Wei, J., Shimazu, J., Makinistoglu, M.P., Maurizi, A., Kajimura, D., Zong, H., Takarada, T., Lezaki, T., Pessin, J.E., Hinoi, E., and Karsenty, G. (2015). Glucose uptake and Runx2 synergize to orchestrate osteoblast differentiation and bone formation. Cell *161*, 1576–1591.
24. Lu, H., Jiang, T., Ren, K., Li, Z.L., Ren, J., Wu, G., and Han, X. (2018). RUNX2 plays an oncogenic role in esophageal carcinoma by activating the PI3K/AKT and ERK signaling pathways. Cell. Physiol. Biochem. *49*, 217–225.
25. Yin, Q., Wang, J., Fu, Q., Gu, S., and Rui, Y. (2018). circRUNX2 through has-miR-203 regulates RUNX2 to prevent osteoporosis. J. Cell. Mol. Med. *22*, 6112–6121.
26. Wang, X., Zhao, B.S., Roundtree, I.A., Lu, Z., Han, D., Ma, H., Weng, X., Chen, K., Shi, H., and He, C. (2015). N^6-methyladenosine modulates messenger RNA translation efficiency. Cell *161*, 1388–1399.
27. Liu, Z., Yao, X., Yan, G., Xu, Y., Yan, J., Zou, W., and Wang, G. (2016). Mediator MED23 cooperates with RUNX2 to drive osteoblast differentiation and bone development. Nat. Commun. *7*, 11149.
28. Tseng, P.C., Hou, S.M., Chen, R.J., Peng, H.W., Hsieh, C.F., Kuo, M.L., and Yen, M.L. (2011). Resveratrol promotes osteogenesis of human mesenchymal stem cells by upregulating RUNX2 gene expression via the SIRT1/FOXO3A axis. J. Bone Miner. Res. *26*, 2552–2563.
29. Li, X., Guo, L., Liu, Y., Su, Y., Xie, Y., Du, J., Zhou, J., Ding, G., Wang, H., Bai, Y., and Liu, Y. (2017). MicroRNA-21 promotes osteogenesis of bone marrow mesenchymal stem cells via the Smad7-Smad1/5/8-Runx2 pathway. Biochem. Biophys. Res. Commun. *493*, 928–933.
30. Liu, Y., Berendsen, A.D., Jia, S., Lotinun, S., Baron, R., Ferrara, N., and Olsen, B.R. (2012). Intracellular VEGF regulates the balance between osteoblast and adipocyte differentiation. J. Clin. Invest. *122*, 3101–3113.
31. Lund, E., and Dahlberg, J.E. (2006). Substrate selectivity of exportin 5 and Dicer in the biogenesis of microRNAs. Cold Spring Harb. Symp. Quant. Biol. *71*, 59–66.
32. Zhang, L., Tang, Y., Zhu, X., Tu, T., Sui, L., Han, Q., Yu, L., Meng, S., Zheng, L., Valverde, P., et al. (2017). Overexpression of miR-335-5p promotes bone formation and regeneration in mice. J. Bone Miner. Res. *32*, 2466–2475.
33. Hu, N., Feng, C., Jiang, Y., Miao, Q., and Liu, H. (2015). Regulative effect of mir-205 on osteogenic differentiation of bone mesenchymal stem cells (BMSCs): possible role of SATB2/Runx2 and ERK/MAPK pathway. Int. J. Mol. Sci. *16*, 10491–10506.
34. Chesnut, C.H., 3rd, Silverman, S., Andriano, K., Genant, H., Gimona, A., Harris, S., Kiel, D., LeBoff, M., Maricic, M., Miller, P., et al.; PROOF Study Group (2000). A randomized trial of nasal spray salmon calcitonin in postmenopausal women with established osteoporosis: the prevent recurrence of osteoporotic fractures study. Am. J. Med. *109*, 267–276.
35. Silva, B.C., and Bilezikian, J.P. (2011). New approaches to the treatment of osteoporosis. Annu. Rev. Med. *62*, 307–322.
36. Wu, X., Pang, L., Lei, W., Lu, W., Li, J., Li, Z., Frassica, F.J., Chen, X., Wan, M., and Cao, X. (2010). Inhibition of Sca-1-positive skeletal stem cell recruitment by alendronate blunts the anabolic effects of parathyroid hormone on bone remodeling. Cell Stem Cell *7*, 571–580.

37. Aghebati-Maleki, L., Dolati, S., Zandi, R., Fotouhi, A., Ahmadi, M., Aghebati, A., Nouri, M., Kazem Shakouri, S., and Yousefi, M. (2019). Prospect of mesenchymal stem cells in therapy of osteoporosis: A review. J. Cell. Physiol. *234*, 8570–8578.

38. Jing, H., Liao, L., An, Y., Su, X., Liu, S., Shuai, Y., Zhang, X., and Jin, Y. (2016). Suppression of EZH2 prevents the shift of osteoporotic MSC fate to adipocyte and enhances bone formation during osteoporosis. Mol. Ther. *24*, 217–229.

39. Wu, Y., Xie, L., Wang, M., Xiong, Q., Guo, Y., Liang, Y., Li, J., Sheng, R., Deng, P., Wang, Y., et al. (2018). Mettl3-mediated m^6A RNA methylation regulates the fate of bone marrow mesenchymal stem cells and osteoporosis. Nat. Commun. *9*, 4772.

40. Li, C.J., Cheng, P., Liang, M.K., Chen, Y.S., Lu, Q., Wang, J.Y., Xia, Z.Y., Zhou, H.D., Cao, X., Xie, H., et al. (2015). MicroRNA-188 regulates age-related switch between osteoblast and adipocyte differentiation. J. Clin. Invest. *125*, 1509–1522.

41. Guo, Q., Chen, Y., Guo, L., Jiang, T., and Lin, Z. (2016). miR-23a/b regulates the balance between osteoblast and adipocyte differentiation in bone marrow mesenchymal stem cells. Bone Res. *4*, 16022.

42. Warda, A.S., Kretschmer, J., Hackert, P., Lenz, C., Urlaub, H., Höbartner, C., Sloan, K.E., and Bohnsack, M.T. (2017). Human METTL16 is a N^6-methyladenosine (m^6A) methyltransferase that targets pre-mRNAs and various non-coding RNAs. EMBO Rep. *18*, 2004–2014.